nature immunology

TCRα-TCRβ pairing controls recognition of CD1d and directs the development of adipose NKT cells

Joshua A Vieth[1,2], Joy Das[3], Fanomezana M Ranaivoson[1,2], Davide Comoletti[1,2,4], Lisa K Denzin[1,2,5–7] & Derek B Sant'Angelo[1,2,5–7]

© 2016 Nature America, Inc., part of Springer Nature. All rights reserved.

The interaction between the T cell antigen receptor (TCR) expressed by natural killer T cells (NKT cells) and the antigen-presenting molecule CD1d is distinct from interactions between the TCR and major histocompatibility complex (MHC). Our molecular modeling suggested that a hydrophobic patch created after TCRα–TCRβ pairing has a role in maintaining the conformation of the NKT cell TCR. Disruption of this patch ablated recognition of CD1d by the NKT cell TCR but not interactions of the TCR with MHC. Partial disruption of the patch, while permissive to the recognition of CD1d, significantly altered NKT cell development, which resulted in the selective accumulation of adipose-tissue-resident NKT cells. These results indicate that a key component of the TCR is essential for the development of a distinct population of NKT cells.

Invariant natural killer T cells (NKT cells), a subset of αβ T cells restricted by the antigen-presenting molecule CD1d, are recognized for their functional diversity and potential roles in autoimmunity, cancer and obesity. These cells express a canonical T cell antigen receptor (TCR) α-chain (variable (V) and joining (J) regions $V_{\alpha}14$-$J_{\alpha}18$) paired with a restricted repertoire of V_{β} chains consisting of $V_{\beta}8.2$, $V_{\beta}7$ or $V_{\beta}2$, with $V_{\beta}8.2$ being most common (roughly 60% of NKT cells)[1]. As potent modulators of the immune system, NKT cells regulate the function of other cell types by rapidly producing both pro-inflammatory cytokines and anti-inflammatory cytokines[2–5]. This duality of effector functions has led to seemingly conflicting biological outcomes. Examples include both tumoricidal activity and tumor-protective activity in mouse models and involvement in both the onset of and protection from liver steatosis in response to a high-fat diet[5–8]. It remains unclear if the particular functions of NKT cells are a result of microenvironment-specific conditioning or if distinct subsets of NKT cells are selected in the thymus.

Unlike conventional αβ TCRs, which recognize peptides presented by the major histocompatibility complex (MHC) molecules, NKT cell TCR heterodimers are restricted to the recognition of lipids presented by the MHC-class-I-like molecule CD1d[9]. The binding of CD1d-glycolipid complexes by NKT cell TCRs has been proposed to be dependent on more rigid complementary-determining regions (CDRs) that result in a 'lock-and-key'-type interaction, in contrast to such binding by conventional TCRs, which seem to require CDR flexibility to adapt to highly polymorphic peptide-MHC complexes[10,11].

It has been argued that the NKT cell TCR functions more like an evolutionary conserved pattern-recognition receptor[12]. Therefore, we considered the possibility that conserved, non–ligand-binding regions of the TCR, possibly domains involved in heterodimer rigidity, might have a direct role in controlling binding to CD1d. Structural analysis revealed an internal hydrophobic patch formed after TCRα–TCRβ heterodimerization that, when disrupted by alteration of the TCRβ chain, substantially affected the recognition of CD1d-glycolipid complexes. Conventional TCRs bearing the same β-chain substitution were, however, still able to functionally interact with MHC class I and MHC class II. Partial disruption of this hydrophobic region, on the other hand, was permissive to CD1d binding but led to the selective development of adipose-resident NKT cells. Thus, our data reveal characteristics of the TCR that can control the development of a distinct subpopulation of NKT cells.

RESULTS

The TCR dimer interface controls recognition of CD1d

Published reports analyzing the crystal structures of NKT cell αβ TCR complexes and single TCRβ chains versus those of ββ TCR homodimers have suggested that the interface between both αβ heterodimers and ββ homodimers relies on five amino acids (TCRβ Tyr35, Gln37, Leu43, Phe91 and Phe108) within the variable domain of the β-chain[13]. The hydrophobic 'patch' or 'pocket' focused on residue Phe108 in the TCRβ chain (TCRβ Phe108) has been hypothesized to be involved in alignment of the β-chain with the α-chain[14]. We analyzed the published structure of the NKT cell TCR ($V_{\alpha}14$-$V_{\beta}8.2$ TCR heterodimer; Protein Data Bank accession code, 3HE6)[15] to determine the localization of this pocket. The amino acid Phe108 is buried within the αβ heterodimeric interface, well removed from the CDR loops

[1]Child Health Institute of New Jersey, Rutgers University, New Brunswick, New Jersey, USA. [2]Rutgers Robert Wood Johnson Medical School, Rutgers University, New Brunswick, New Jersey, USA. [3]Immunology Program, Sloan-Kettering Institute, Memorial Sloan-Kettering Cancer Center, New York, New York, USA. [4]Department of Neuroscience and Cell Biology, Rutgers University, New Brunswick, New Jersey, USA. [5]Rutgers Graduate School of Biomedical Sciences, Rutgers University, New Brunswick, New Jersey, USA. [6]Department of Pediatrics, Rutgers University, New Brunswick, New Jersey, USA. [7]Department of Pharmacology, Rutgers University, New Brunswick, New Jersey, USA. Correspondence should be addressed to D.B.S. (santandb@rwjms.rutgers.edu).

Received 13 July; accepted 21 October; published online 21 November 2016; doi:10.1038/ni.3622

© 2016 Nature America, Inc., part of Springer Nature. All rights reserved.

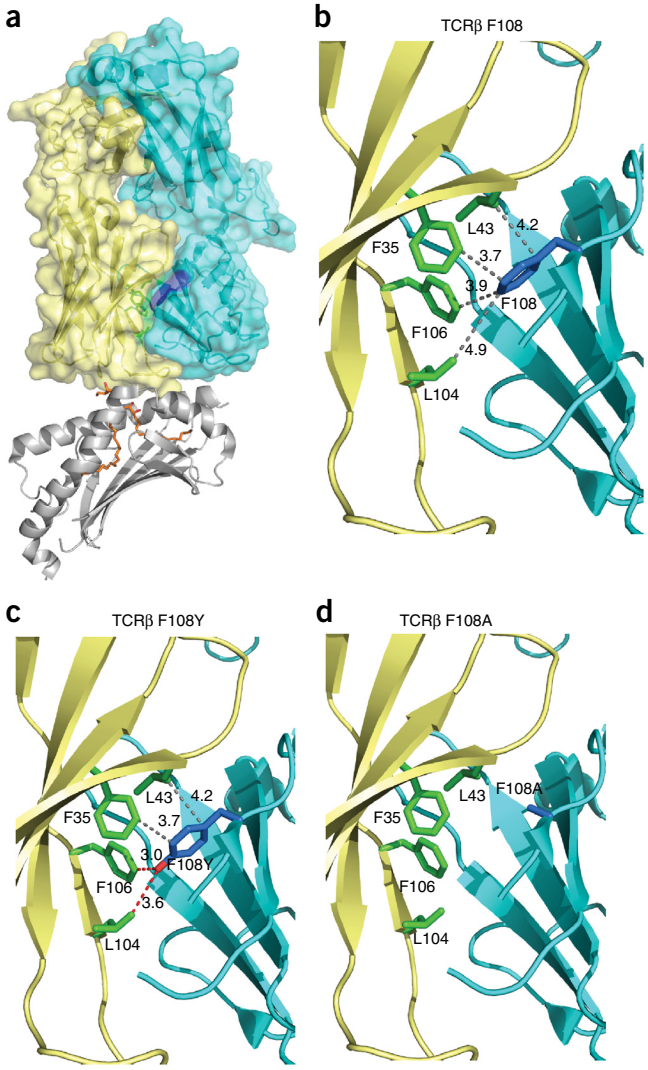

Figure 1 Analysis of a hydrophobic 'patch' formed by pairing of the TCR α- and β-chains. (**a**) Structure of CD1d loaded with α-galactosylceramide and the mouse $V_α14$-$V_β8.2$ NKT cell TCR (Protein Data Bank accession code, 3HE6)[15], showing the hydrophobic pocket focused on Phe108 (dark blue) of the β-chain (light blue) and the α-chain (yellow). (**b**) Residues in the structure in **a** (TCRα Leu43 (L43), Phe35 (F35), Phe106 (F106) and Leu104 (L104) (green); TCRβ Phe108 (F108) (dark blue)) that form the hydrophobic pocket between the α-chain and β-chain (dark blue); numbers along dashed lines indicate the distance (in angstroms) between Phe108 of the β-chain and the interacting residues of the α-chain. (**c**) A structure as in **b** with the TCRβ F108Y substitution, with exposure of the hydroxyl group (red) that is hypothesized to interfere with the hydrophobic pocket in the vicinity of Phe106 and Leu104 of the α-chain. (**d**) A structure as in **b** with the TCRβ F108A substitution, which is hypothesized to disrupt the hydrophobic contacts with all four α-chain residues.

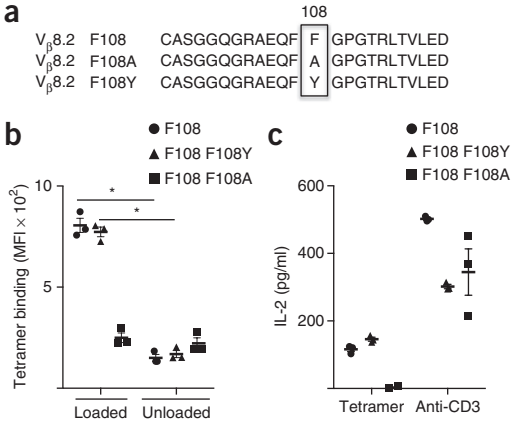

Figure 2 The hydrophobic pocket of the NKT cell TCR heterodimer is essential for the recognition of CD1d. (**a**) Sequences of wild-type and mutant variants of $V_β8.2$; outlined area indicates replacement of Phe108. (**b**) Flow cytometry analysis of the binding of soluble fluorescence-labeled CD1d-Tet loaded with α-galactosylceramide (Loaded) or unloaded (control) CD1d tetramers (horizontal axis) by cells (1×10^4 per sample) stably transfected to express the invariant $V_α14$-$J_α28$ TCRα chain plus TCRβ Phe108 (F108), TCRβ F108Y or TCRβ F108A (key), presented as mean fluorescence intensity (MFI). (**c**) ELISA of IL-2 in cells as in **b** (key) stimulated with plate-bound monoclonal antibody (2C11) to CD3 or plate-bound CD1d-Tet loaded with PBS57 (horizontal axis). Each symbol (**b**,**c**) represents an individual sample; small horizontal lines indicate the mean (±s.e.m.). $^*P < 0.05$ (two-sided *t*-test). Data are representative of three independent experiments.

that interact with CD1d (**Fig. 1a**), and is accommodated by four residues (TCRα Leu43, Phe35, Phe106 and Leu104) on the TCRα chain (**Fig. 1b**).

We performed molecular modeling of substitution of tyrosine for the phenylalanine at position 108 of TCRβ (TCRβ F108Y) in the $V_α14$-$V_β8.2$ structure (Protein Data Bank accession code, 3HE6). Inclusion of the tyrosine polar hydroxyl group was considered likely to destabilize the hydrophobic pocket due to spatial separation in the vicinity of TCRα Leu104 and TCRα Phe106 while presumably keeping the contacts involving the aromatic ring (**Fig. 1c**). Modeling of replacement of the phenylalanine at position 108 of TCRβ with alanine (TCRβ F108A) suggested that all four molecular contacts made by the Phe108 side chain within the hydrophobic pocket would be lost, which would possibly lead to changes of the quaternary structure of the αβ heterodimer that, in turn, could affect the function of the receptor (**Fig. 1d**).

To test the effect of such substitutions on the binding of ligand, we transfected the TCR$^-$ mouse thymoma cell line 4G4 (ref. 16) with vector encoding the invariant $V_α14$-$J_α28$ TCRα chain and co-transfected it with vector encoding either wild-type TCRβ (with Phe108: TCRβ F108) or TCR $V_β8.2$ containing the point substitutions described above (TCRβ F108Y or TCRβ F108A)[17] (**Fig. 2a**). Clones with similar surface expression of the TCR were selected by flow cytometry on the basis of staining with antibody to CD3ε (part of the TCR complex). The ability of each of these TCRs to bind soluble fluorescence-labeled CD1d tetramers loaded with the α-galactosylceramide analog PBS157 (ref. 18) (CD1d-Tet) was assessed by flow cytometry. The binding of the tetramers to wild-type TCRβ F108 and mutant TCRβ F108Y was indistinguishable, as indicated by the mean fluorescence intensity (**Fig. 2b**). However, the binding of CD1d-Tet to TCRβ F108A was nearly identical to the binding of unloaded (control) tetramers to TCRβ F108A (**Fig. 2b**), which indicated that specific binding of CD1d-Tet to TCRβ F108A was abolished.

To assess the functionality of the cell lines transfected to express the mutant TCRβ F108Y and TCRβ F108A chains relative to that of cells lines expressing wild-type TCRβ F108, we used plate-bound CD1d-Tet to measure antigen-specific activation. Consistent with the tetramer-binding data, production of the cytokine IL-2 was lost in cells transfected to express TCRβ F108A, in contrast to its production by those expressing the wild-type TCRβ F108, indicative of a complete

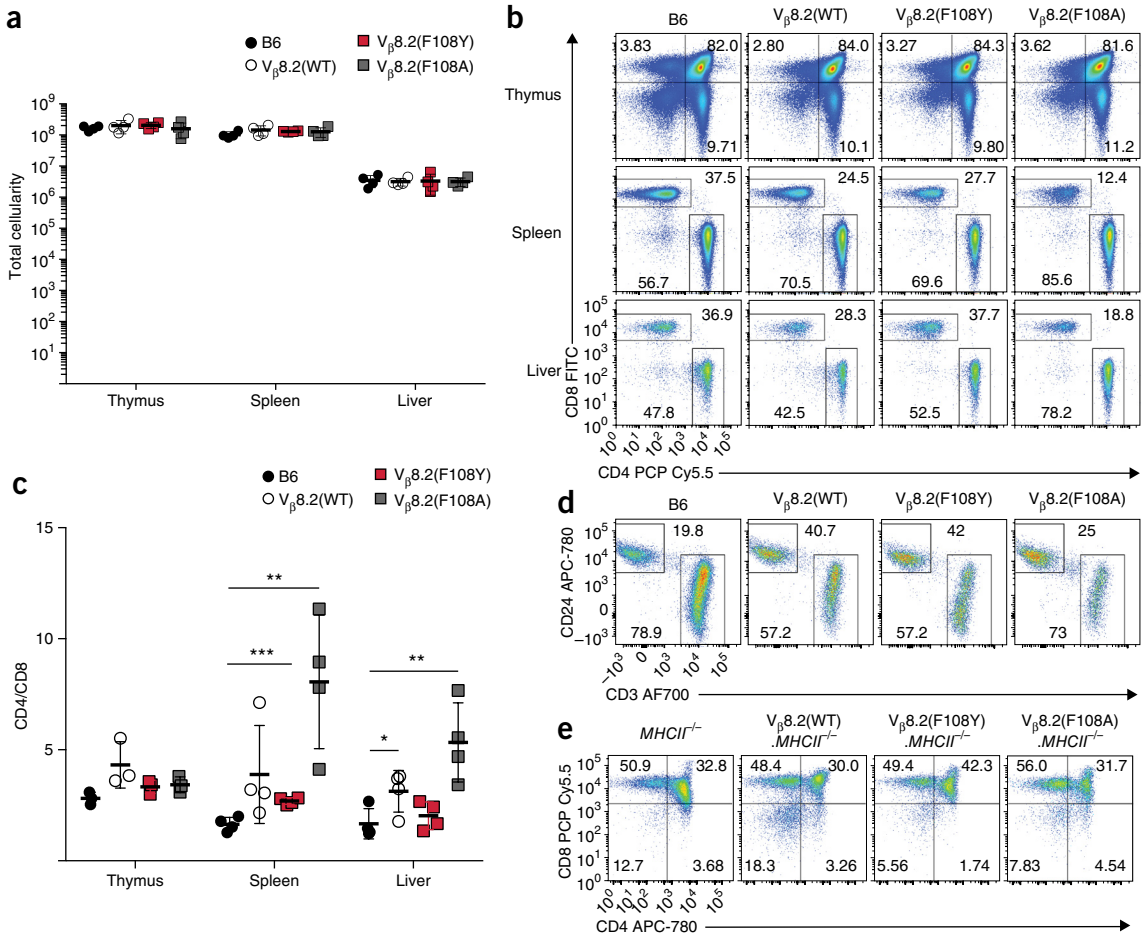

Figure 3 Disruption of the F108Y hydrophobic patch is permissive for conventional T cell development. (**a**) Total cellularity of the thymus, spleen and liver of B6, V_β8.2(WT), V_β8.2(F108Y) and V_β8.2(F108A) mice ($n = 4$ per genotype; key), assessed by light microscopy with a hemocytometer, with trypan blue staining used for the exclusion of non-viable cells. (**b**) Flow cytometry of DAPI$^-$MHCII$^-$ populations from the thymus, spleen and liver of mice as in **a** (above plots), showing results for total thymocytes (top row) or only CD3$^+$ T cells (middle and bottom). Numbers in quadrants (top row) indicate percent cells in each (throughout); numbers adjacent to outlined areas (middle and bottom rows) indicate percent CD8$^+$CD4$^-$ (CD8SP) cells (top left) or CD8$^-$CD4$^+$ (CD4SP) cells (bottom right). (**c**) Ratio of the frequency of CD4$^+$ T cells to the frequency of CD8$^+$ T cells (CD4/CD8) in the CD3$^+$ population of mice as in **a** ($n = 4$ per genotype). (**d**) Flow cytometry of MHCII$^-$CD8$^+$ thymocytes of mice as in **a**. Numbers adjacent to outlined areas indicate percent CD24$^+$CD3$^-$ cells (top left) or CD24$^-$CD3$^+$ cells (bottom right). (**e**) Flow cytometry of CD3^{hi} thymocytes (1×10^5 per sample) in *MHCII*$^{-/-}$, V_β8.2(WT).*MHCII*$^{-/-}$, V_β8.2(F108Y).*MHCII*$^{-/-}$ and V_β8.2(F108A).*MHCII*$^{-/-}$ mice (above plots). Each symbol (**a**,**c**) represents an individual mouse; small horizontal lines indicate the mean (±s.e.m.). Not significant in **a** ($P > 0.05$); $^*P < 0.05$, $^{**}P < 0.01$ and $^{***}P < 0.001$ (two-tailed *t*-test). Data are from three independent experiments with four biological replicates (**a**–**c**) or three experiments with three biological replicates (**d**,**e**).

© 2016 Nature America, Inc., part of Springer Nature. All rights reserved.

loss of CD1d-mediated activation, while the cells transfected to express TCRβ F108Y retained the ability to produce IL-2 in response to CD1d (**Fig. 2c**). Notably, the hybridomas expressing wild-type TCRβ F108 or mutant TCRβ F108Y or TCRβ F108A all produced IL-2 in response to plate-bound anti-CD3 (**Fig. 2c**). Combined, these data indicated that the point substitutions at Phe108 that affected the TCRα–TCRβ heterodimer interface did not disrupt TCRα–TCRβ dimerization but altered the specific recognition of CD1d-presented ligands by the canonical V_α2-V_β8.2 NKT cell TCR.

The TCRβ Phe108 substitution permits T cell development

To test the efficacy of TCRs using the mutant TCRβ F108A and TCRβ F108Y chains *in vivo*, we generated mice with transgenic expression of each TCRβ chain on a background with homozygous deficiency in the TCR β-chain constant region (V_β8.2(F108Y) and V_β8.2(F108A), respectively). As control, we used a mouse line with transgenic expression of the wild-type V_β8.2 region of the TCR β-chain on that same background (V_β8.2(WT))[16,19]. The TCR expression of each strain of mouse was similar to that of wild-type C57BL/6 (B6) mice (**Supplementary Fig. 1a**). Overall cellularity in the thymus, spleen and liver was similar in B6 (control) mice and the V_β8.2(WT), V_β8.2(F108Y) and V_β8.2(F108A) mice (**Fig. 3a**). Analysis of the CD4$^+$ or CD8$^+$ T cell populations from the thymus, spleen and liver of B6, V_β8.2(WT), V_β8.2(F108Y) and V_β8.2(F108A) mice by flow cytometry showed that selection by MHC class I and MHC class II was intact in each strain (**Fig. 3b**). We observed modest skewing toward the development of CD4$^+$ T cells in V_β8.2(WT) and V_β8.2(F108Y) mice and especially in V_β8.2(F108A) mice, relative to that in B6 (control) mice (**Fig. 3c**), which suggested possible disruption of the development of CD8$^+$ T cells. To exclude this possibility, we verified by flow cytometry that the CD8$^+$ single-positive (CD8SP) thymocytes were not CD8$^+$CD3$^-$CD24^{hi} intermediate single-positive cells. After we eliminated intermediate single-positive cells from the analysis, a distinct CD24$^-$CD3$^+$ population of CD8SP cells remained (**Fig. 3d**), indicative of proper MHC-class-I-mediated

selection. To further confirm the development of CD8SP cells, we generated Vβ8.2(WT), Vβ8.2(F108Y) and Vβ8.2(F108A) mice with homozygous deficiency in the locus encoding MHC class II (*H2*$^{-/-}$; called '*MHCII*$^{-/-}$' here: Vβ8.2(WT).*MHCII*$^{-/-}$, Vβ8.2(F108Y).*MHCII*$^{-/-}$ and Vβ8.2(F108A).*MHCII*$^{-/-}$ mice, respectively). Total thymocytes from age-matched *MHCII*$^{-/-}$, Vβ8.2(WT).*MHCII*$^{-/-}$, Vβ8.2(F108Y).*MHCII*$^{-/-}$ and Vβ8.2(F108A).*MHCII*$^{-/-}$ mice were stained for the monomorphic co-receptors CD4 and CD8. CD8SP thymocytes were observed, but CD4$^+$ single-positive thymocytes were not (**Fig. 3e**), which indicated that the CD8SP thymocytes and CD8$^+$ T cells observed in these mice were not an aberrant MHC-class-II-restricted population. Together these data showed that TCRs expressing the TCRβ F108Y or TCRβ F108A substitution were able to associate with MHC class I and MHC class II in the Vβ8.2(F108Y) and Vβ8.2(F108A) mice, which resulted in the development of both CD4$^+$ T cells and CD8$^+$ T cells.

Expression of the cell-surface marker CD24 and activation marker CD69 on thymocytes and CD3$^+$ T cells in the spleen of Vβ8.2(WT), Vβ8.2(F108Y) and Vβ8.2(F108A) mice was also similar to their expression in B6 (control) mice (**Supplementary Fig. 1b**). Additionally, CD25$^+$CD4$^+$ regulatory T cells, which, like NKT cells, are thought to require strong TCR signaling for development[20], were also present at a normal frequency in the Vβ8.2(F108Y) and Vβ8.2(F108A) mice relative to their frequency in Vβ8.2(WT) and B6 (control) mice (**Supplementary Fig. 1c**). Finally, the effect of the TCRβ F108Y or TCRβ F108A substitution on TCR Vα pairing was assessed in CD4$^+$ or CD8$^+$ T cells from the spleen. The four different Vα chains detectable by flow cytometry were expressed at the surface of CD4$^+$ or CD8$^+$ T cells from Vβ8.2(F108Y) and Vβ8.2(F108A) mice (**Supplementary Fig. 2**), which demonstrated proper pairing with the mutant TCRβ chains. Together these data showed that the TCRs with substitution of TCRβ Phe108 were able to productively interact with MHC class I and MHC class II.

Disruption of NKT cell development

We next determined whether substitution of the Phe108 pocket was permissive to CD1d-mediated selection of NKT cells. Consistent with the *in vitro* binding data, no CD3$^+$CD1d-Tet$^+$ NKT cells were detected at an abundance above that of cells stained with unloaded control tetramers in the thymus, spleen or liver of Vβ8.2(F108A) mice (**Fig. 4a**,**b** and **Supplementary Fig. 3a**). Unexpectedly, although mutant TCRβ F108Y bound CD1d-tet similarly to wild-type TCRβ Phe108, the frequency of CD3$^+$CD1d-Tet$^+$ NKT cells was much lower in the thymus, spleen and liver of Vβ8.2(F108Y) mice than in those of B6 mice (**Fig. 4a**,**b**). As previously reported[19], the Vβ8.2(WT) mice expressing the wild-type form of TCR Vβ8.2 had a greater frequency of NKT cells in the thymus, spleen and liver than that of B6 mice (**Fig. 4a**,**b**).

To address the possibility that the CD1d-Tet reagent might not have been able to detect NKT cells in the Vβ8.2(F108A) mice, we analyzed the frequency of CD3$^+$NK1.1$^+$ NKT cells by flow cytometry. We observed significantly smaller CD3$^+$NK1.1$^+$ populations in the thymus, spleen and liver of Vβ8.2(F108Y) and Vβ8.2(F108A) mice than in those of B6 mice (**Supplementary Fig. 3b**). This suggested that the reduction and ablation (respectively) of CD1d-Tet$^+$ NKT cells was not due to an inability to identify the cells with the CD1d-Tet reagent. Together these data showed that the partial or complete disruption of the TCR Vβ Phe108 hydrophobic patch diminished the frequency of or ablated the NKT cell population in Vβ8.2(F108Y) mice and Vβ8.2(F108A) mice, respectively.

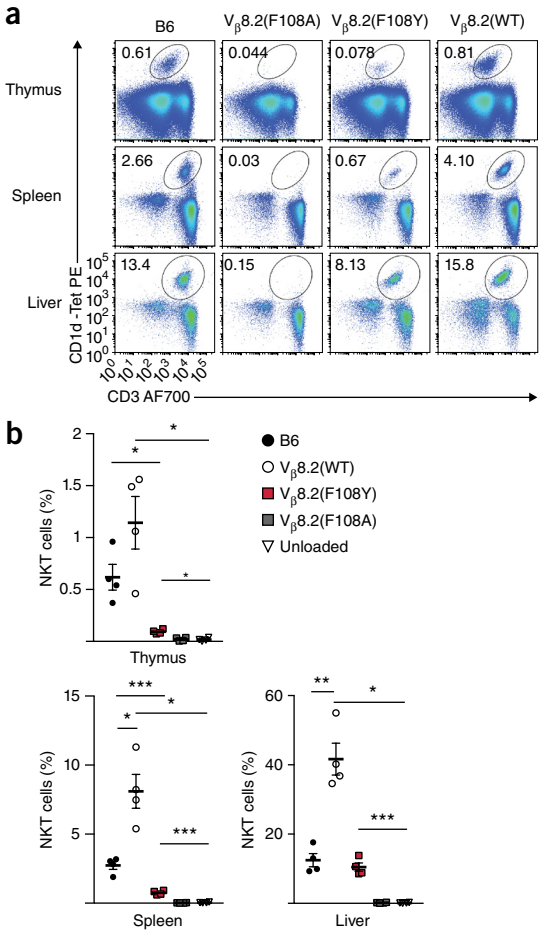

Figure 4 Substitution of TCRβ Phe108 disrupts NKT cell development. (**a**) Flow cytometry of DAPI$^-$MHCII$^-$ populations from the thymus, spleen and liver of B6, Vβ8.2(WT), Vβ8.2(F108Y) and Vβ8.2(F108A) mice. Numbers adjacent to outlined areas indicate percent CD3$^+$ cells that bound PBS57-loaded CD1d-Tet (NKT cells). (**b**) Quantification of NKT cells in the thymus, spleen and liver of mice as in **a** ($n = 4$ per genotype), presented as the frequency of CD3$^+$ cells (1×10^5 per sample) that bound PBS57-loaded CD1d-Tet or unloaded CD1d tetramer (B6 mice only) (key). Each symbol (**b**) represents an individual mouse; small horizontal lines indicate the mean (±s.e.m.). $^*P < 0.05$, $^{**}P < 0.01$ and $^{***}P < 0.001$ (Mann-Whitney *U*-test). Data are from four independent experiments with four biological replicates.

Induction of adipose NKT cell development by TCRβ F108Y

We next assessed NKT cells in the thymus of Vβ8.2(F108Y) mice to determine if partial disruption of the TCRβ Phe108 pocket altered their development. Thymic CD3$^+$CD1d-Tet$^+$ NKT cells from Vβ8.2(F108Y) mice were largely CD44^{lo}NK1.1^{lo} (**Fig. 5a**) and predominantly CD24$^+$ (**Fig. 5b**), whereas CD3$^+$CD1d-Tet$^+$ populations from the thymus of age-matched Vβ8.2(WT) and B6 (control) mice were predominantly CD44^{hi}NK1.1^{hi} (**Fig. 5a**) and CD24$^-$ (**Fig. 5b**). The transcription factor PLZF is essential for the development of NKT cells and their effector functions[21,22]. PLZF expression was much lower in thymic CD3$^+$CD1d-Tet$^+$ NKT cells from Vβ8.2(F108Y) mice than in those from Vβ8.2(WT) or B6 (control) mice (**Fig. 5c**). When this analysis was limited to 'mature' CD44$^+$NK1.1$^+$ thymic NKT cells, lower PLZF expression was also observed in cells from Vβ8.2(F108Y) mice than in similar cells from wild-type B6 or Vβ8.2(WT) mice (**Fig. 5c**).

© 2016 Nature America, Inc., part of Springer Nature. All rights reserved.

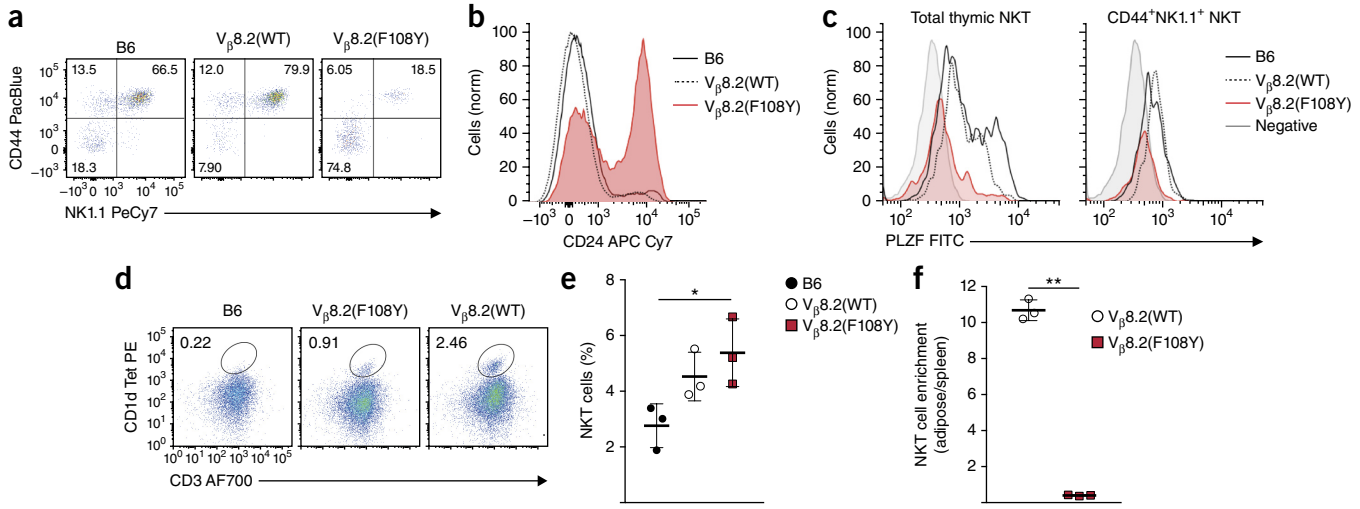

Figure 5 The TCRβ F108Y substitution alters NKT cell development and induces the development of adipose-resident NKT cells. (**a**) Flow cytometry analysis of the expression of CD44 and NK1.1 on sorted tetramer-positive NKT cell populations (1×10^4 per sample) from B6, V_β8.2(WT) and V_β8.2(F108Y) mice, assessing the development of NKT cells. (**b**) CD24 expression by total thymic NKT cells (1×10^5 per sample) from B6, V_β8.2(WT) and V_β8.2(F108Y) mice; results are normalized (norm) to the mode. (**c**) PLZF expression in sorted total thymic NKT cells (left) or CD44$^+$NK1.1$^+$ mature NKT cells (right) from B6, V_β8.2(WT) and V_β8.2(F108Y) mice (1×10^4 cells per sample) (normalized as in **b**); CD8SP thymocytes serve as a negative control. (**d**) Flow cytometry of epididymal CD45.2$^+$MHCII$^-$ cells (single cells) from the adipose tissue of B6, V_β8.2(WT) and V_β8.2(F108Y) mice. Numbers adjacent to outlined areas indicate percent CD3$^+$ cells that bound CD1d-tet (NKT cells). (**e**) Quantification of adipose-resident NKT cells as in **d** ($n = 4$ mice per genotype), presented as the frequency of cells in the CD3$^+$ population that bound CD1d-tet. (**f**) Ratio of adipose-resident NKT cells in V_β8.2(WT) or V_β8.2(F108Y) mice (relative to that of B6 mice) to spleen-resident NKT cells (relative to that of B6 mice) ($n = 3$ mice per group). Each symbol (**e**,**f**) represents an individual mouse; small horizontal lines indicate the mean (±s.e.m.). $^*P < 0.01$ and $^{**}P < 0.001$ (Mann-Whitney *U*-test). Data are from three independent experiments with three biological replicates.

The unusual phenotype of the V_β8.2(F108Y) thymic NKT cells was reminiscent of published data on the phenotype of adipose-resident NKT cells[23]. To determine if the acquisition of an adipose-tissue-like phenotype by NKT cells during thymic development in V_β8.2(F108A) mice resulted in trafficking to adipose tissue, we analyzed the CD3$^+$CD1d-Tet$^+$ NKT cell populations in the epididymal adipose tissue of V_β8.2(WT) and V_β8.2(F108Y) mice by flow cytometry. The adipose tissue of V_β8.2(F108A) mice was not included because of the complete lack of NKT cells in these mice. In contrast to the lower frequency of NKT cells in the thymus, spleen and liver of V_β8.2(F108Y) mice than in those of B6 (control) mice, the frequency of CD3$^+$CD1d-Tet$^+$ NKT cells in the adipose tissue of V_β8.2(F108Y) mice was approximately 5.5% of the total CD3$^+$ cells, compared with a frequency of approximately 2.5% of the CD3$^+$ cells in the adipose tissue of B6 (control) mice (**Fig. 5d**,**e**). Consistent with their larger CD3$^+$CD1d-Tet$^+$ NKT populations in all tissues, V_β8.2(WT) mice also had greater frequency of CD1d-Tet$^+$ NKT cells among total CD3$^+$ cells in the adipose tissue than did B6 (control) mice (**Fig. 5d**,**e**). To control for the systemic greater abundance of NKT cells in V_β8.2(WT) mice[19], we determined the absolute number of CD3$^+$CD1d-Tet$^+$ NKT cells per gram of adipose tissue in V_β8.2(F108Y) or V_β8.2(WT) mice and then normalized those results to changes in splenic NKT populations. This analysis showed an 11-fold greater number of NKT cells per gram of adipose tissue relative to changes in the spleen of V_β8.2(F108Y), compared with a 0.13-fold greater number in V_β8.2(WT) mice (**Fig. 5f**), suggestive of 'preferential' homing of NKT cells to the adipose tissue of V_β8.2(F108Y) mice.

Acquisition of the adipose-resident phenotype in the thymus

Adipose-resident cells NKT are reported to have several similarities to regulatory T cells[23,24]. For example, the inhibitory receptor PD-1 had high expression specifically on adipose-resident CD3$^+$CD1d-Tet$^+$ NKT cells (**Fig. 6a**,**b**). Consistent with data obtained for wild-type mice, a substantial frequency of NKT cells from V_β8.2(WT) mice and V_β8.2(F108Y) mice also expressed PD-1 on CD3$^+$CD1d-Tet$^+$ NKT cells isolated from adipose tissue (**Fig. 6a**,**b**). However, PD-1 expression was not detected on thymic CD3$^+$CD1d-Tet$^+$ NKT cells from B6 or V_β8.2(WT) mice (**Fig. 6a**,**b**). In contrast, however, 15–20% of CD3$^+$CD1d-Tet$^+$ thymic NKT cells from the V_β8.2(F108Y) mice were PD-1$^+$ (**Fig. 6a**,**b**).

The transcription factor E4BP4 (Nfil3), which controls transcription of the gene encoding IL-10 in regulatory T cells[24], is also specifically expressed by adipose-resident NKT cells[23]. E4BP4 seems to be essential for the regulatory functions of adipose-resident NKT cells, since knocking down E4BP4 diminishes IL-10 production[23]. Intracellular staining of CD3$^+$CD1d-Tet$^+$ NKT cells from the adipose tissue and thymus of B6 mice showed that E4BP4 was expressed only in the NKT cells from adipose tissue (**Fig. 6c**,**d**). Once again, CD3$^+$CD1d-Tet$^+$ NKT cells from the thymus of V_β8.2(F108Y) were found to be different. There was a significant upregulation of 1.2-fold in the expression of E4BP4 in thymic NKT cells in V_β8.2(F108Y) mice relative to its expression in such cells from B6 (control) or V_β8.2(WT) mice (**Fig. 6c**,**d**). Analysis of the hepatic CD3$^+$CD1d-Tet$^+$ NKT cell population showed that E4BP4 expression was not higher in these cells in V_β8.2(F108Y) mice than in such cells from B6 or V_β8.2(WT) mice (data not shown). Splenic NKT cells were not analyzed due to their extremely small populations in the V_β8.2(F108Y) mice. These data suggested that partial disruption of the Phe108 hydrophobic contacts in the NKT cell TCR heterodimer resulted in altered development of NKT cells in V_β8.2(F108Y) mice and induced an adipose-tissue-like phenotype during thymic development.

Homing of NKT cells to adipose tissue in V_β8.2(F108Y) mice

To investigate whether NKT cells in V_β8.2(F108Y) mice had a competitive advantage for accumulation in adipose tissue, we established

© 2016 Nature America, Inc., part of Springer Nature. All rights reserved.

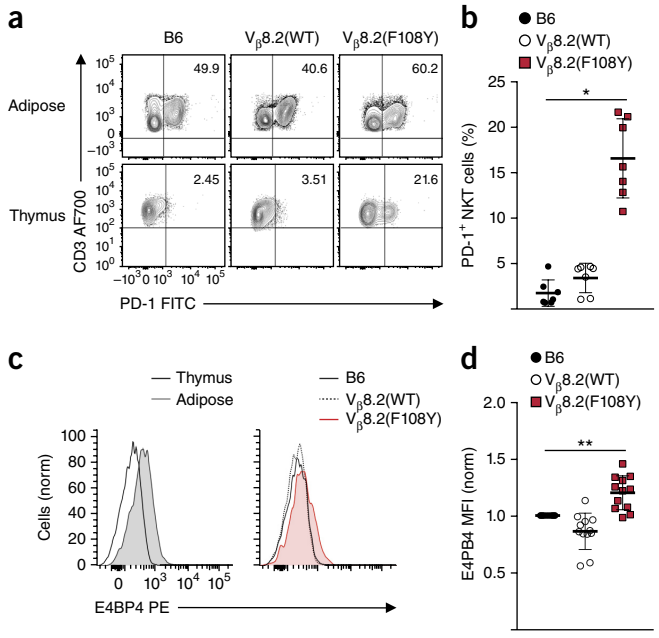

Figure 6 Thymic NKT cells express adipose-related markers. (**a**) Flow cytometry of NKT cells from the adipose tissue and thymus (left margin) of B6, V_β8.2(WT) and V_β8.2(F108Y) mice. Numbers in top right quadrants indicate percent CD3$^+$PD-1$^+$ cells. (**b**) PD-1 expression in NKT cells from the thymus of B6, V_β8.2(WT) and V_β8.2(F108Y) mice ($n = 7$ per genotype). (**c**) E4BP4 expression in NKT cells from the thymus or adipose tissue of B6 mice (left) and thymic NKT cells from B6, V_β8.2(WT) and V_β8.2(F108Y) mice (right) (results normalized as in **Fig. 5b**). (**d**) Mean fluorescence intensity of E4BP4 in NKT cells from the thymus of B6, V_β8.2(WT) and V_β8.2(F108Y) mice ($n = 12$ per genotype); results are normalized to those of B6 mice. Each symbol (**b**,**d**) represents an individual mouse; small horizontal lines indicate the mean (±s.e.m.). $*P < 0.01$ and $**P < 0.001$ (Mann-Whitney *U* test). Data are from four independent experiment with seven biological replicates (**a**,**b**) or five independent experiments with twelve biological replicates (**c**,**d**), with 2×10^3 cells per sample (thymus) or 3×10^2 cells per sample (adipose) in each.

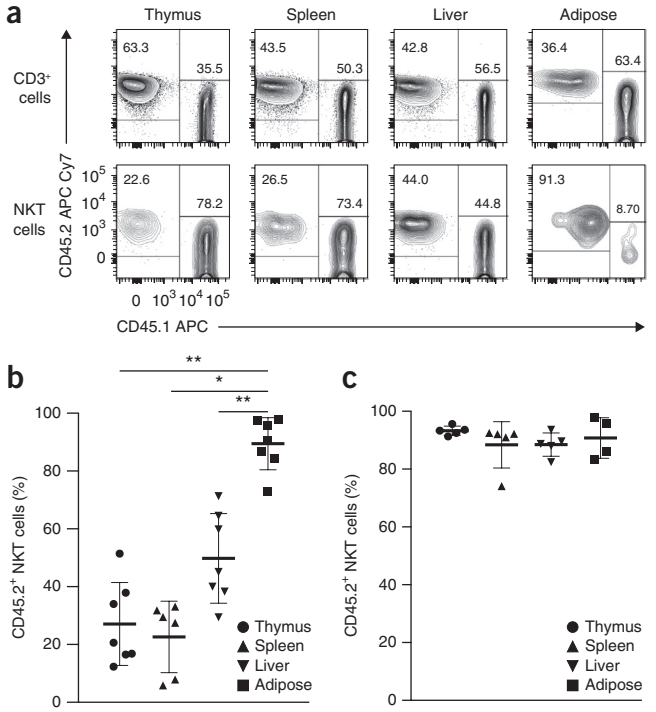

Figure 7 NKT cells expressing TCRβ F108Y acquire an adipose-like phenotype in the thymus. (**a**) Flow cytometry of cells from *Rag1*$^{-/-}$(B6.SJL/V_β8.2(F108Y)) mixed-bone-marrow chimeras, showing the contribution of total CD3$^+$ T cells and CD3$^+$CD1d-Tet$^+$ NKT cells derived from B6.SJL (CD45.1$^+$) or V_β8.2(F108Y) (CD45.2$^+$) donor mice at 10 weeks after transplantation. Numbers adjacent to outlined areas indicate percent CD45.2$^+$ (V_β8.2(F108Y)) cells (top left) or CD45.1$^+$ (B6.SJL) cells (bottom right). (**b**) Frequency of CD45.2$^+$ NKT cells (derived from V_β8.2(F108Y) donor mice) in the thymus, spleen, liver and adipose tissue of *Rag1*$^{-/-}$ host mice ($n = 6$ (spleen) or $n = 7$ (thymus, liver and adipose tissue)). (**c**) Frequency of CD45.2$^+$ NKT cells (derived from V_β8.2(WT) donor mice) in the thymus, spleen, liver and adipose tissue of *Rag1*$^{-/-}$(B6.SJL/V_β8.2(WT)) mixed-bone-marrow chimeras ($n = 5$ (thymus, spleen and liver) or $n = 4$ (adipose tissue)). Each symbol (**b**,**c**) represents an individual mouse; small horizontal lines indicate the mean (±s.e.m.). $*P < 0.01$ and $**P < 0.001$ (Mann-Whitney *U* test). Data are from three independent experiments with four (**c**, adipose tissue), five (**d**, thymus, spleen and liver), six (**b**, spleen) or seven (**b**, thymus, liver and adipose tissue) biological replicates, and with 1.5×10^5 CD3$^+$ cells (thymus and spleen), 2.5×10^3 CD3$^+$ cells (liver), 1×10^3 CD3$^+$ cells (adipose tissue), 2×10^3 NKT cells (spleen, thymus and liver) or 1×10^2 NKT cells (adipose tissue).

mixed-bone-marrow chimeras by injecting equal numbers of magnetically sorted c-Kit$^+$Lin$^-$ cells from the bone marrow of C57BL/6.SJL (B6.SJL) (CD45.1$^+$) mice and either V_β8.2(F108Y) (CD45.2$^+$) mice or V_β8.2(WT) (CD45.2$^+$) mice into sublethally irradiated T cell–deficient (*Rag1*$^{-/-}$) host mice (to generate *Rag1*$^{-/-}$(B6.SJL/V_β8.2(F108Y)) mice and *Rag1*$^{-/-}$(B6.SJL/V_β8.2(WT)) mice, respectively). The reconstitution of conventional CD3$^+$ T cells from each donor in *Rag1*$^{-/-}$(B6.SJL/V_β8.2(F108Y)) chimeras was similar in the thymus, spleen, liver and adipose tissue 10 weeks after transplantation, as determined by expression of the congenic markers CD45.1 and CD45.2 (**Fig. 7a**,**b**). As expected, few (20–25%) of the CD3$^+$CD1d-Tet$^+$ NKT cells in the thymus and spleen of *Rag1*$^{-/-}$(B6.SJL/V_β8.2(F108Y)) mice were derived from V_β8.2(F108Y) (CD45.2$^+$) mice. In contrast, CD3$^+$CD1d-Tet$^+$ NKT cells derived from V_β8.2(F108Y) mice accounted for almost the entire population in the adipose tissue (**Fig. 7a**,**b**). The frequency CD45.1$^+$ CD3$^+$CD1d-Tet$^+$ NKT cells in the liver of *Rag1*$^{-/-}$(B6.SJL/V_β8.2(F108Y)) mice was similar to that of their CD45.2$^+$ counterparts (**Fig. 7a**,**b**). In contrast, and consistent with published data, V_β8.2(WT) cells were present at a substantial frequency (approximately 90%) in all tissues of *Rag1*$^{-/-}$(B6.SJL/V_β8.2(WT)) mice and exhibited no selective recruitment to adipose tissue (**Fig. 7c**). Overall, these data indicated that the adipose-like phenotype of thymic NKT cells induced by expression of the TCRβ F108Y mutant resulted in specific enrichment of NKT cells in the adipose tissue.

Altered signaling by TCRβ F108Y

The lineage specification of developing thymocytes has been associated with differential signaling through the TCR due to the avidity of ligand binding. Thus, we investigated if the changes in the development of NKT cells in TCRβ F108Y mice were due to altered ligand-TCR interactions during positive selection. When assessed by flow cytometry, binding of CD1d-Tet loaded with the high-affinity α-galactosylceramide analog PBS57 or with the α-galactosylceramide analog OCH (of comparatively lower affinity) by CD3$^+$CD1d-Tet$^+$ NKT cells from the liver of B6, V_β8.2(WT) and V_β8.2(F108Y) mice was similar (**Supplementary Fig. 4a**). Next, we incubated CD1d-Tet-labeled hepatic NKT cells from B6, V_β8.2(WT) and V_β8.2(F108Y)

© 2016 Nature America, Inc., part of Springer Nature. All rights reserved.

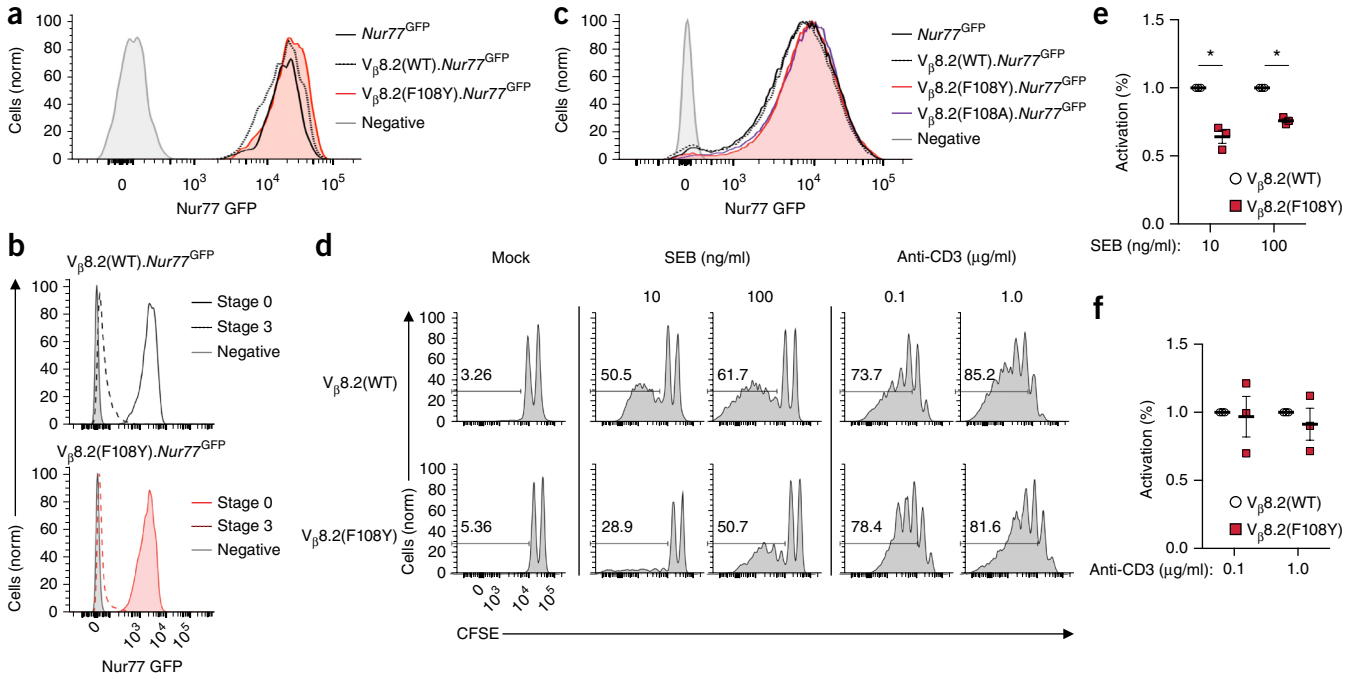

Figure 8 TCR signaling is mediated by the TCRβ F108Y substitution. (**a**) GFP (Nur77) expression in stage 0 ($CD3^+CD1d\text{-}Tet^+CD44^-$ $NK1.1^-CD24^+$) NKT cells sorted from *Nur77*^{GFP}, $V_\beta8.2(F108Y).Nur77^{GFP}$ and $V_\beta8.2(F108A).Nur77^{GFP}$ mice (key) (results normalized as in **Fig. 5b**); corresponding populations from GFP-negative littermates serve as a negative control. (**b**) GFP (Nur77) expression in stage 0 and stage 3 ($CD44^+NK1.1^+CD24^-$) NKT cells (key) sorted from $V_\beta8.2(WT).Nur77^{GFP}$ mice (top) and $V_\beta8.2(F108Y).Nur77^{GFP}$ mice (bottom); negative control as in **a**, and normalized as in **a**). (**c**) GFP (Nur77) expression in thymocytes that had undergone positive TCR selection ($CD69^{hi}$) from *Nur77*^{GFP}, $V_\beta8.2(WT).Nur77^{GFP}$, $V_\beta8.2(F108Y).Nur77^{GFP}$ and $V_\beta8.2(F108A).Nur77^{GFP}$ mice (key); negative control as in **a**, and normalized as in **a**. (**d**) CFSE dilution by $CD3^+$ T cells isolated from the spleen of $V_\beta8.2$(WT) and $V_\beta8.2$(F108Y) mice and activated *in vitro* for 72 h with SEB (0 (Mock), 10 or 100 ng/ml) or anti-CD3 (0.1 or 1 μg; control), assessed by flow cytometry (normalized as in **a**). Numbers above bracketed lines indicate percent proliferated ($CFSE^{lo}$) cells. (**e**) Activation of T cells obtained from $V_\beta8.2$(WT) and $V_\beta8.2$(F108Y) mice ($n = 3$) and cultured *in vitro* with SEB (**e**) or anti-CD3 (**f**) as in **d**; results were normalized to those of cells from $V_\beta8.2$(WT) mice and are presented as the frequency of activated T cells. Each symbol (**e**,**f**) represents an individual mouse; small horizontal lines indicate the mean (±s.e.m.). $^*P < 0.01$ (two-tailed *t* test). Data are from three independent experiments with three biological replicates, and with 4×10^3 $CD3^+$ T cells per sample.

mice with soluble tetramer and increasing concentrations of competing antibody and assessed the avidity of each TCR for CD1d-Tet by a CD1d-Tet–decay assay that measures the dissociation of CD1d-Tet by flow cytometry. A similar loss of fluorescence due to dissociation of CD1d-Tet, roughly 50% in blocking antibody at a concentration of 100 μg/ml, was observed for all three strains of mice (**Supplementary Fig. 4b**). While these data indicated that the avidity of NKT cells expressing TCRβ F108Y for CD1d-lipid ligands was not much different from that of NKT cells expressing wild-type TCRβ F108, the binding of α-galactosylceramide-loaded CD1d-Tet is not equivalent to the binding of endogenous CD1d-ligand complexes during T cell development. To assess TCR signaling during development *in vivo*, we crossed the $V_\beta8.2$(WT), $V_\beta8.2$(F108Y) and $V_\beta8.2$(F108A) mice with *Nur77*^{GFP} mice, which express green fluorescent protein (GFP) from the gene encoding the nuclear hormone receptor Nur77 (ref. 25), to generate $V_\beta8.2(WT).Nur77^{GFP}$, $V_\beta8.2(F108Y).Nur77^{GFP}$ and $V_\beta8.2(F108A).Nur77^{GFP}$ mice. GFP expression in *Nur77*^{GFP} T cells has been shown to correlate with the strength of signaling through the TCR. Immature stage 0 NKT cells, which are $CD44^-NK1.1^-CD24^{hi}$, have higher GFP expression than that of more-mature NKT cell populations[25], most probably due to TCR signaling associated with positive selection. Comparison of thymic $CD44^-NK1.1^-CD24^{hi}$ stage 0 NKT cells by flow cytometry showed similar expression of GFP in both $V_\beta8.2(WT).Nur77^{GFP}$ mice and $V_\beta8.2(F108Y).Nur77^{GFP}$ mice and the *Nur77*^{GFP} (control) mice (**Fig. 8a**), indicative of similar TCR-mediated signaling at this stage. In addition, thymic $CD44^+NK1.1^+$ stage 3 $CD1d\text{-}Tet^+$ NKT cells showed lower expression of GFP in $V_\beta8.2(WT).Nur77^{GFP}$ and $V_\beta8.2(F108Y).Nur77^{GFP}$ mice, similar to that in *Nur77*^{GFP} (control) mice (**Fig. 8b**). Among total, non-NKT cell $CD69^{hi}$ thymocytes, GFP expression was upregulated similarly in $V_\beta8.2(WT).Nur77^{GFP}$, $V_\beta8.2(F108Y).Nur77^{GFP}$ and $V_\beta8.2(F108A).Nur77^{GFP}$ mice relative to its expression in such cells from *Nur77*^{GFP} (control) mice (**Fig. 8c**). Since CD69 expression is a marker for TCR signaling in conventional thymocytes following productive interactions of the TCR with MHC during positive selection, these data indicated that the positive selection of conventional thymocytes was not perturbed by the TCRβ Phe108 substitutions. Together these data suggested that the altered development of NKT cells in the $V_\beta8.2$(F108Y) mice was not due to changes in TCR signaling strength during selection or changes in the ability to bind CD1d-ligand complexes.

Finally, we sought to determine if the TCRβ F108Y substitution might have a role in altered signaling independently of ligand binding. *Staphylococcus aureus* enterotoxin B (SEB) is a functional superantigen that activates nearly all T cells expressing $V_\beta8$ TCRs directly through the TCR V_β region[26]. Thus, SEB can activate $V_\beta8.2$-expressing T cells via the TCR, independently of antigen-specific MHC interactions. We labeled total splenocytes from $V_\beta8.2$(WT) and $V_\beta8.2$(F108Y) mice with the division-tracking dye CFSE and activated the cells for 3 d in serum-supplemented medium containing SEB at a concentration

© 2016 Nature America, Inc., part of Springer Nature. All rights reserved.

of 0, 10 or 100 ng/ml, then assessed the cells by flow cytometry. The $CD3^+$ T cells from V_β8.2(F108Y) mice showed less proliferation in response to SEB than did the $CD3^+$ T cells from V_β8.2(WT) mice, particularly at the low dose of SEB (10 ng/ml) (**Fig. 8d**,**e**). The proliferation of $CD3^+$ T cells from V_β8.2(WT) mice was similar to that of $CD3^+$ T cells from V_β8.2(F108Y) mice, following activation with anti-CD3ε (clone 145-2C11) at a concentration of either 0.1 μg/ml or 1 μg/ml (**Fig. 8d**,**f**). Therefore, although direct binding of ligands by TCRβ F108Y was not compromised, and CD1d- and MHC-mediated signaling during development was intact, the activation of T cells by superantigen binding to the TCR was lower in T cells expressing the TCRβ F108Y mutant. Overall, these data indicated that signaling specific to the TCRβ chain has a role in the selection of NKT subpopulations.

DISCUSSION

The unusual interaction of the NKT cell TCR with its CD1d ligands has been compared with the evolutionarily conserved recognition of pathogen-associated molecular patterns by innate immunological receptors[12]. Here we have explored how hydrophobic contacts between the TCRα and TCRβ chains might influence the recognition of CD1d and the development and function of invariant NKT cells. Combined, our data have shown that complete alteration of this region of the TCR ablated ligand recognition, while partial disruption substantially altered the development of NKT cells.

Interestingly, alteration of that TCR motif resulted in the induction of several key features of adipose-resident NKT cells during thymic development. The distinct phenotype and function of adipose-resident NKT cells was potentially a consequence of microenviromentally induced alterations of typical NKT cells. However, our data indicated that signals received in the thymus directed the development of these cells. Therefore, rather than having an induced phenotype, adipose-resident NKT cells are probably a distinct cell type. Consistent with the naming convention used for $CD8^+$ tissue-resident memory T cells ('T_{RM} cells'), follicular helper T cells ('T_{FH} cells') and others, we suggest that the adipose-resident NKT cell lineage be called 'arNKT cells'.

Despite its substantial effect on NKT cell development, the alteration to the TCR did not measurably alter the binding of CD1d-ligand complexes or diminish TCR signaling. It is possible that ligand discrimination during thymic development is exceptionally subtle or at least more subtle than our ability to directly measure such interactions. How ligand binding triggers the activation of T cells has proven to be a complex problem that is still poorly understood, particularly in terms of the relaying of ligand-specific information through the TCR during development. If altered signaling that is below detection were directing development of this distinct lineage, this would raise the possibility that a very minor progression of changes in TCR-ligand interactions might be involved in defining a multitude of different effector functions. Alternatively, our data showed changes in activation via a superantigen, which raised the possibility that the commitment of developing NKT cells into distinct lineages might be dependent on more than simply the binding avidity of the NKT cell TCR for CD1d-ligand complexes. Perhaps, as is the case for helper T cells, TCR-associated proteins such as CD4 and specific isoforms of CD45 can affect the sensitivity of ligand detection[27]. The hydrophobic-patch alteration might have prevented the recruitment of other proteins because it blocked a conformational change in the αβ TCR, similar to the hypothesis of Janeway[27,28]. If the αβ heterodimer itself was not affected, it is possible that the reorganization of CD3ζ subunits, which has been shown to be necessary for the potentiation of ligand-specific TCR signaling, was affected[29,30]. Such studies indicate that binding of ligand by the TCR ectodomain can result in phosphorylation of the cytoplasmic domains of the CD3 subunits. This raises the possibility that altering interactions between the TCRα and TCRβ chains via the TCRβ F108Y substitution during the binding of CD1d-ligand complexes could have influenced the assembly of the dimeric signaling modules (CD3δε, CD3γε and CD3ζζ). Whatever the precise mechanism, our studies have shown that altered recognition of ligands selects for T cells with distinct functional characteristics. Overall, these results have identified an important, highly conserved feature of the TCR that is essential for the recognition of CD1d-presented ligands and that controls the functional development of NKT cells.

METHODS

Methods, including statements of data availability and any associated accession codes and references, are available in the online version of the paper.

Note: Any Supplementary Information and Source Data files are available in the online version of the paper.

ACKNOWLEDGMENTS

We thank L. Osorio for technical assistance; R. Worth and V. Shapiro for review of the manuscript; A. Roberts for cell sorting; A. Laouar (Rutgers University) for the *Rag1*$^{-/-}$ mice; the late C. Janeway (Yale University School of Medicine) for the 4G4 cell line; T. Novak (Yale University) for the pMCFR vector; and the US National Institutes of Health Tetramer Core for the CD1d-PBS57 and CD1d-OCH tetramer reagents. Supported by the NIAID of the US National Institutes of Health (R01 AI083988 and AI059739 to D.B.S.), the NIMH of the US National Institutes of Health (MH092906 and NSF BRAIN EAGER MCB-1450895 to D.C.), the New Jersey Commission on Cancer Research Fellowship and Century for the Cure (Fellowship in Translational Immunology to J.A.V.) and by the Robert Wood Johnson Foundation (67038 to the Child Health Institute of New Jersey).

AUTHOR CONTRIBUTIONS

J.A.V. and D.B.S. designed the study, interpreted data and wrote the manuscript; J.A.V. performed most of the experiments; J.D. generated the cells transfected to express the Phe108 TCR and performed the initial binding and signaling studies; F.M.R. and D.C. assisted with the modeling of the TCR; L.K.D. assisted with data analysis and interpretation; and D.B.S. developed the V_β8.2(F108A), V_β8.2(F108A) mice and V_β8.2(WT) mice.

COMPETING FINANCIAL INTERESTS

The authors declare no competing financial interests.

Reprints and permissions information is available online at http://www.nature.com/reprints/index.html.

1. Bendelac, A., Killeen, N., Littman, D.R. & Schwartz, R.H. A subset of $CD4^+$ thymocytes selected by MHC class I molecules. *Science* **263**, 1774–1778 (1994).
2. Bendelac, A., Savage, P.B. & Teyton, L. The biology of NKT cells. *Annu. Rev. Immunol.* **25**, 297–336 (2007).
3. Brigl, M. & Brenner, M.B. CD1: antigen presentation and T cell function. *Annu. Rev. Immunol.* **22**, 817–890 (2004).
4. Kronenberg, M. Toward an understanding of NKT cell biology: progress and paradoxes. *Annu. Rev. Immunol.* **23**, 877–900 (2005).
5. Taniguchi, M., Harada, M., Kojo, S., Nakayama, T. & Wakao, H. The regulatory role of Valpha14 NKT cells in innate and acquired immune response. *Annu. Rev. Immunol.* **21**, 483–513 (2003).
6. Martin-Murphy, B.V. *et al.* Mice lacking natural killer T cells are more susceptible to metabolic alterations following high fat diet feeding. *PLoS One* **9**, e80949 (2014).
7. Rakhshandehroo, M. *et al.* CD1d-mediated presentation of endogenous lipid antigens by adipocytes requires microsomal triglyceride transfer protein. *J. Biol. Chem.* **289**, 22128–22139 (2014).
8. Yang, W. *et al.* NKT cell exacerbation of liver metastases arising from melanomas transplanted into either the eyes or spleens of mice. *Invest. Ophthalmol. Vis. Sci.* **52**, 3094–3102 (2011).
9. Bendelac, A. CD1: presenting unusual antigens to unusual T lymphocytes. *Science* **269**, 185–186 (1995).
10. Borg, N.A. *et al.* CD1d-lipid-antigen recognition by the semi-invariant NKT T-cell receptor. *Nature* **448**, 44–49 (2007).

© 2016 Nature America, Inc., part of Springer Nature. All rights reserved.

11. Sidobre, S. *et al.* The T cell antigen receptor expressed by Valpha14i NKT cells has a unique mode of glycosphingolipid antigen recognition. *Proc. Natl. Acad. Sci. USA* **101**, 12254–12259 (2004).
12. Scott-Browne, J.P. *et al.* Germline-encoded recognition of diverse glycolipids by natural killer T cells. *Nat. Immunol.* **8**, 1105–1113 (2007).
13. Zhou, B. *et al.* A conserved hydrophobic patch on Vβ domains revealed by TCRβ chain crystal structures: Implications for pre-TCR dimerization. *Front. Immunol.* **2**, 5 (2011).
14. Chothia, C., Boswell, D.R. & Lesk, A.M. The outline structure of the T-cell alpha beta receptor. *EMBO J.* **7**, 3745–3755 (1988).
15. Pellicci, D.G. *et al.* Differential recognition of CD1d-α-galactosyl ceramide by the V β 8.2 and V β 7 semi-invariant NKT T cell receptors. *Immunity* **31**, 47–59 (2009).
16. Sant'Angelo, D.B. *et al.* The specificity and orientation of a TCR to its peptide-MHC class II ligands. *Immunity* **4**, 367–376 (1996).
17. Hong, S.C. *et al.* An MHC interaction site maps to the amino-terminal half of the T cell receptor α chain variable domain. *Cell* **69**, 999–1009 (1992).
18. Liu, Y. *et al.* A modified α-galactosyl ceramide for staining and stimulating natural killer T cells. *J. Immunol. Methods* **312**, 34–39 (2006).
19. Dao, T. *et al.* Development of CD1d-restricted NKT cells in the mouse thymus. *Eur. J. Immunol.* **34**, 3542–3552 (2004).
20. Kronenberg, M. & Rudensky, A. Regulation of immunity by self-reactive T cells. *Nature* **435**, 598–604 (2005).
21. Savage, A.K. *et al.* The transcription factor PLZF directs the effector program of the NKT cell lineage. *Immunity* **29**, 391–403 (2008).
22. Kovalovsky, D. *et al.* The BTB-zinc finger transcriptional regulator PLZF controls the development of invariant natural killer T cell effector functions. *Nat. Immunol.* **9**, 1055–1064 (2008).
23. Lynch, L. *et al.* Regulatory iNKT cells lack expression of the transcription factor PLZF and control the homeostasis of $T_{(reg)}$ cells and macrophages in adipose tissue. *Nat. Immunol.* **16**, 85–95 (2015).
24. Motomura, Y. *et al.* The transcription factor E4BP4 regulates the production of IL-10 and IL-13 in $CD4^+$ T cells. *Nat. Immunol.* **12**, 450–459 (2011).
25. Moran, A.E. *et al.* T cell receptor signal strength in Treg and iNKT cell development demonstrated by a novel fluorescent reporter mouse. *J. Exp. Med.* **208**, 1279–1289 (2011).
26. Kappler, J. *et al.* V beta-specific stimulation of human T cells by staphylococcal toxins. *Science* **244**, 811–813 (1989).
27. Novak, T.J. *et al.* Isoforms of the transmembrane tyrosine phosphatase CD45 differentially affect T cell recognition. *Immunity* **1**, 109–119 (1994).
28. Janeway, C.A. Jr. Ligands for the T-cell receptor: hard times for avidity models. *Immunol. Today* **16**, 223–225 (1995).
29. Lee, M.S. *et al.* A mechanical switch couples T cell receptor triggering to the cytoplasmic juxtamembrane regions of CD3ζζ. *Immunity* **43**, 227–239 (2015).
30. Xu, C., Call, M.E. & Wucherpfennig, K.W. A membrane-proximal tetracysteine motif contributes to assembly of CD3deltaepsilon and CD3gammaepsilon dimers with the T cell receptor. *J. Biol. Chem.* **281**, 36977–36984 (2006).

© 2016 Nature America, Inc., part of Springer Nature. All rights reserved.

ONLINE METHODS

Mice. All animal work was performed in compliance with the Rutgers University Internal Animal Care and Use Committee (IACUC) and the guidelines of the Federal Office of Laboratory Animal Welfare. C57BL/6 mice, C57BL/6.SJL mice, MHC-class-II-deficient mice, *Nur77*^{GFP} mice and mice deficient in the TCR β-chain constant region were purchased from Jackson Laboratories. V_β8.2(WT) mice have been previously described[19]. *Rag1*$^{-/-}$ mice were provided by A. Laouar (Rutgers University). V_β8.2 transgenes were generated by PCR and cloned into the hCD2 vector by use of the In-Fusion kit (Clontech). The transgene was isolated away from the plasmid vector by gel electrophoresis and prepared for microinjection. Transgenes were injected directly into fertilized C57BL/6 zygotes. At least two founders were generated for each line. Transgenes were introduced by breeding into C57BL/6 mice deficient in the TCR β-chain constant region. For each experiment, animals were age matched, and whenever possible, control littermates were used. No selection within experiments was made with regard to animal sex, and no other randomization was used.

Structural analysis of the NKT cell TCR. A published sequence of the V_α14-V_β8.2 NKT cell TCR bound to α-galactosylceramide presented by CD1d (Protein Data Bank accession code, 3HEJ)[15], as well as variations containing point substitutions at Phe108 of the β chain were analyzed using PyMOL software for the prediction of tertiary structure.

Cells transfected to express TCRs. Mutations in sequence encoding the wild-type TCRβ chain were generated by PCR, cloned and sequenced. The 4G4 cell line was originally obtained from C. Janeway (Yale University School of Medicine). The cell line was authenticated by flow cytometry and verified to be mycoplasma free by PCR. Transfections into 4G4 cells were done by electroporation of a pMCFR vector originally provided by T. Novak (Yale University), which provides a high expression in T cells. Selection was performed by G418. Clones were generated by limiting dilution. Transfectants were activated either with plate-bound anti-CD3 (2C11) (BD Biosciences, 1 μg/ml) or PBS57-loaded tetramer (NIH Tetramer Core Facility, 1:500) for approximately 16 h. IL-2 production was measured using an ELISA kit (BD) according to the manufacturers recommendations.

Tetramer-binding assays. 4G4 cells expressing the invariant NKT cell TCRα chain and either of the TCR V_β8.2 substitutions or non-mutant V_β8.2 as a control were labeled with soluble phycoerythrin-tagged PBS57-CD1d tetramers provided by the NIH Tetramer Core Facility. Mean fluorescence intensity (MFI) was determined by flow cytometry. Unloaded CD1d tetramers were used as a negative control. For tetramer-decay assays, NKT cells from the liver were isolated using an autoMACS Pro Separator (Miltenyi Biotec) as described below, and labeled with anti-CD3 and PBS57-loaded tetramer. Following labeling, cells were incubated in PBS supplemented with 1% FBS (HyClone) and 0, 10, 50, 100 or 200 μg/ml anti-TCR V_β8 (F23.1) (BD Pharm) blocking antibody for 2 h at room temperature with gentle pipetting every 30 min to maintain the cells in suspension. Flow cytometry was performed, and tetramer binding at each concentration of blocking antibody was determined by the MFI of binding of the PBS57-CD1d tetramer divided by the MFI of anti-CD3. Tetramer decay was calculated by normalizing each sample to the 0 μg/ml control.

Preparation of lymphocytes from tissue samples. Single-cell suspensions were prepared by dissociation of whole tissues between glass slides and passage through a 40-μm mesh filter. For splenocytes and thymocytes, red blood cell lysis was performed using Red Blood Cell Lysing Buffer (Sigma, St. Louis, MO) and remaining cells were counted on a haemacytometer. For hepatocytes, the homogenate was suspended in Percoll (Sigma, St. Louis, MO) to a final concentration of 30% Percoll supplemented with 10 units/ml heparin. Hepatocytes were then centrifuged for 30 min at 2,000 r.p.m. in a Sorvall RTH-750 rotor. Lymphocytes were then collected from the buffy layer, washed once with stain buffer and counted on a hemocytometer. For the isolation of fat lymphocytes, epididymal fat pads were collected from each mouse and weighed and then minced with a scalpel. Samples were then incubated in complete media containing 1 mg/ml Collagenase Type IV (Sigma) and 1% Fetal Bovine Serum (HyClone) rotating at 37 °C for 25 min. Adipose-resident lymphocytes were then isolated by washing once with RPMI and once with PBS, and filtering through a 40-μm mesh filter.

Flow cytometry and cell sorting. Single-cell suspensions were incubated with normal mouse serum, unlabeled streptavidin, and Fc-receptor-blocking antibody before being stained on ice with specific antibodies and tetramer. For staining with anti-PLZF antibody, cells were made permeable with an intracellular staining buffer set (eBioscience). For surface staining, dead cells were excluded from analysis by use of the DNA-binding dye DAPI (4,6-diamidino-2-phenylindole). Cell doublets were excluded by comparison of side-scatter width to forward-scatter area. Gating strategies for the identification of populations referenced in the manuscript are provided (**Supplementary Fig. 5**) Sorting of NKT cells was performed on an autoMACS Pro Separator (Miltenyi Biotec). Cells were labeled with NKT-cell-TCR-specific tetramer labeled with phycoerythrin (PE) followed by PE-specific microbeads (Miltenyi Biotec) before separation, and analyzed for purity after sorting. Samples were collected on a LSR II maintained by the Sant'Angelo laboratory (BD Biosciences) using FACSDiva software, and analyzed with FlowJo version 10 software (Tree Star). Antibodies conjugated to fluorescein isothiocyanate, phycoerythrin, peridinine chlorophyll protein complex 5.5, allphycocyanin, phycoerythrin-cyanine 7, allphycocyanin-cyanine 7, allophycocyanin-efluor 780, pacific blue, alexa-fluor 488, alexa-fluor 700, alexa-fluor 594, or alexa-fluor 647 were used as follows: from BD Biosciences (anti-CD3 (500A2, 1:500), anti-CD4 (RM45, 1:1,000) and anti-CD8a (53-6.7, 1:500)); from eBioscience (anti-CD45.2 (104, 1:1,000), anti-NK1.1 (PK136, 1:500), anti-CD24 (M1/69, 1:500), anti-PD-1 (J43, 1:200) and E4BP4 (S2M-E19, 1:300)); from BioLegend (anti-CD44 (IM7, 1:500) and anti-CD45.1(A20, 1:300)); or produced and labeled by the Monoclonal Antibody Core Facility of Memorial Sloan-Kettering Cancer Center (anti-MHC class II (212.A1, 1:1,000) and anti-PLZF (Mags.21F7, 1:500)). Tetramers of PBS57-CD1d were provided by the US National Institutes of Health Tetramer Core Facility and used as previously described[21]. Tetramers not loaded with PBS57 were used a negative and background controls to eliminate nonspecific events.

Mixed bone marrow chimeras. c-Kit$^+$ cells were sorted from whole bone marrow of V_β8.2(F108A) (CD45.2$^+$) mice, V_β8.2(WT) (CD45.2$^+$) mice and B6.SJL (CD45.1$^+$) mice using c-Kit (CD117) MicroBeads and an autoMACS Pro Separator (Miltenyi Biotec). 1:1 mixtures of c-Kit$^+$ cells from V_β8.2(F108A) and B6.SJL or V_β8.2(WT) and B6.SJL mice were transplanted by i.v. injection (10^6 cells/per recipient) into sublethally irradiated *Rag1*$^{-/-}$ mice (n = 7 mice receiving V_β8.2(F108A) and B6.SJL donor cells, and n = 5 mice receiving V_β8.2(WT) and B6.SJL donor cells). For irradiation, 600 rads of total body irradiation was administered 8 h before injection. 10 weeks after transplantation, thymus, spleen, liver, and adipose tissue was harvested, and total CD3$^+$ cell and NKT cell populations were analyzed by flow cytometry for expression of CD45.1 and CD45.2.

SEB activation. T cells from the spleens of V_β8.2(WT) and V_β8.2(F108A) mice were isolated by AutoMACS (described above) and labeled with CFSE (Life Technologies) according to the protocol provided by the supplier. Following labeling, cells were incubated in complete RPMI Media (Mediatech) supplemented with 1 × Penicillin/Streptomycin Solution (Mediatech) and 5% FBS (HyClone) for 72 h at 37 °C. Activation of T cells was performed adding 10 or 100 ng/ml Staphylococcal Enterotoxin B (SEB) (Toxin Technology, Inc.) or 1 μg/ml anti-CD3 (clone 145-2C11) (BD Biosciences). Changes in CFSE levels were assessed by flow cytometry as describe above.

Statistics. Statistical analysis was performed using Prism Software (GraphPad). Statistical differences were determined with the Student's t-test or Mann-Whitney U-test, a parametric alternative to the Student's t-test that is more robust for small sample sizes[21,22]. For analysis of the mixed-bone-marrow-chimera experiments, two-way ANOVA was used. Error bars represented indicate s.d. from the mean. For all experiments, significance was defined as $^*P < 0.05$, $^{**}P < 0.01$, $^{***}P < 0.001$ and $^{****}P < 0.0001$.

Data availability statement. Further information regarding data and reagents used is available by request to the corresponding author.

© 2016 Nature America, Inc., part of Springer Nature. All rights reserved.

doi:10.1038/ni.3622

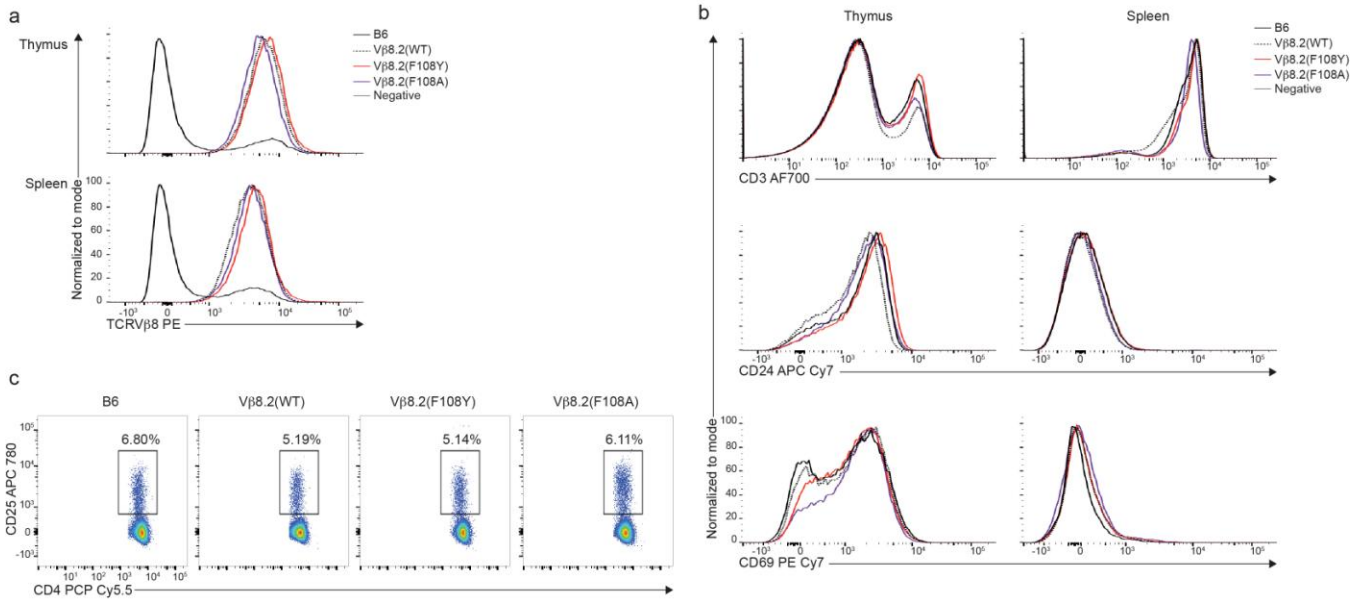

Supplementary Figure 1

T cells in V_β8.2(WT), V_β8.2(F108Y) and V_β8.2(F108A) mice develop similarly to T cells from wild-type mice.

(**a**) Representative histogram showing expression of TCR Vβ8 on the surface of $CD3^{hi}$ cells from the thymus and spleen of B6, V_β8.2(WT), V_β8.2(F108Y), and V_β8.2(F108A) mice. Data are representative of at least three individual experiments and three biological replicates. (**b**) Comparison of T cells from B6, V_β8.2(WT), V_β8.2(F108Y), and V_β8.2(F108A) mice by: expression of CD3 on $DAPI^-$ MHC^- thymocytes and splenocytes (top row), expression of CD24 on $DAPI^-MHC\ II^-CD3^+$ thymocytes and splenocytes (middle row), and expression of CD69 on $DAPI^-MHC\ II^-CD3^{hi}$ thymocytes and splenocytes (bottom row). Data shown are representative of three individual experiments representing three biological replicates. $1x10^4$ target cells analyzed per sample. (**c**) Representative FACS analysis of $DAPI^-MHC\ II^-CD3^+CD4^+$ cells for $CD25^+$ regulatory T cell populations in splenocytes from B6, V_β8.2(WT), V_β8.2(F108Y), and V_β8.2(F108A) mice. Data are representative of three individual experiments representing a total of three biological replicates. $5x10^3$ cells analyzed per sample.

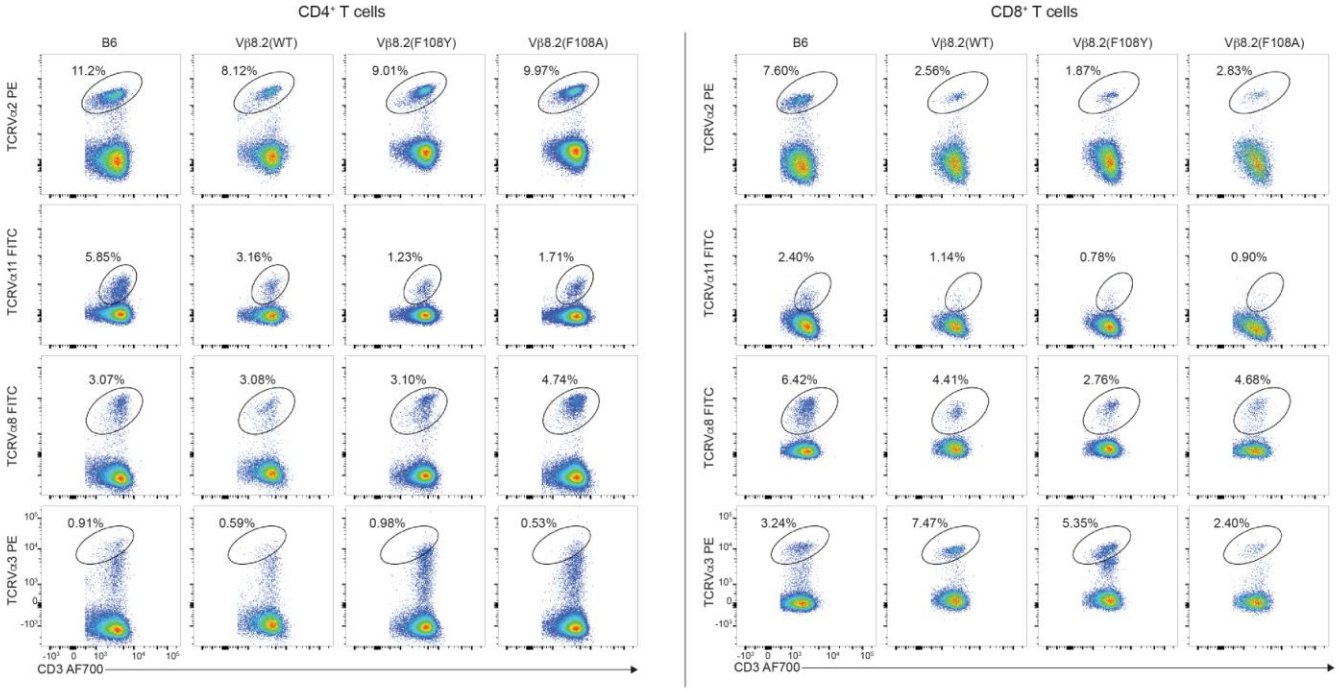

Supplementary Figure 2

The wild-type TCRβ and mutant TCRβ F108Y and TCRβ F108A TCR V_β chains dimerize with multiple V_α segments.

Flow cytometry analysis of splenic DAPI$^-$MHC II$^-$CD3$^+$ T cells stained for CD4 and CD8 expression as well as TCRVα3, TCRVα8, TCRVα11, and TCRVα2 antibodies. Data shown for expression of TCRVα chains in CD4$^+$ (left) and CD8$^+$ (right) T cells separately. 1x10^4 DAPI$^-$MHC II$^-$CD3$^+$ T cells analyzed for each sample, data is representative of three individual experiments assessing a total of three biological replicates.

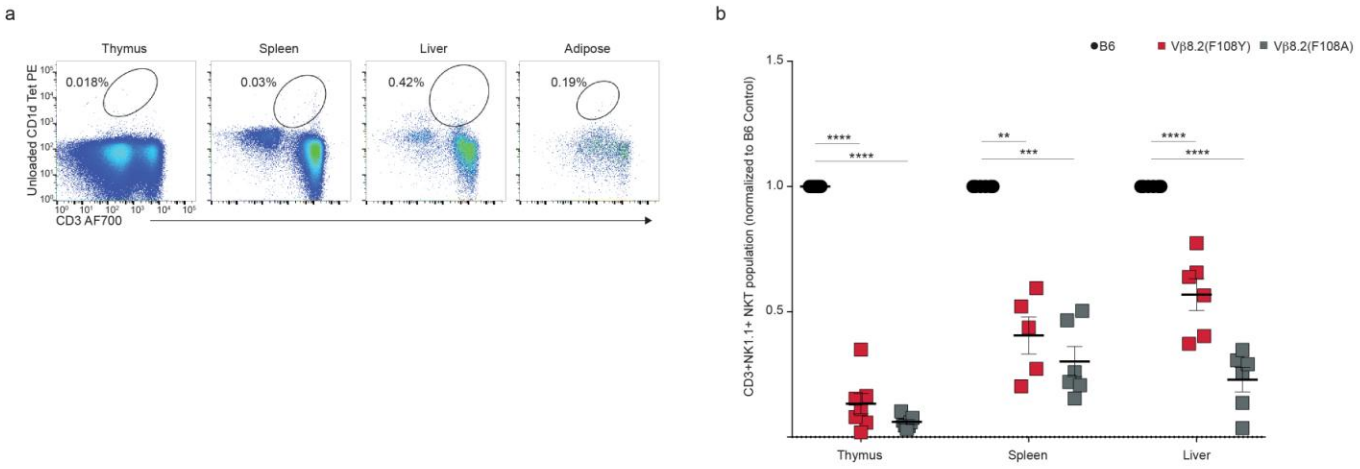

Supplementary Figure 3

Validation of CD1d-Tet flow cytometry for NKT cell populations.

(**a**) Representative flow cytometry showing unloaded CD1d tetramer utilized as a negative control to identify background staining in all the thymus, spleen, liver, and adipose tissue of B6 mice. (**b**) Quantitation of flow cytometry data of the CD3+NK1.1+ total NKT cells in DAPI-MHC II- populations in the thymus, spleen, and liver of B6, V_β8.2(F108Y), and V_β8.2(F108A) mice, normalized to B6 control. (*n*=6 for thymus, spleen, and liver of B6 and V_β8.2(F108A) mice, thymus and liver of V_β8.2(F108Y) mice; *n*=5 for spleen of V_β8.2(F108Y) mice). ***P*<0.01,****P*<0.001, *****P*<0.0001 (Mann-Whitney *U* test). $1x10^4$ $DAPI^-MHC\ II^-$ cells analyzed for each sample. Data derived from three combined experiments representing a total of five (**b**, V_β8.2(F108A) splenocytes only) or six biological replicates (mean ±s.e.m. in **b**).

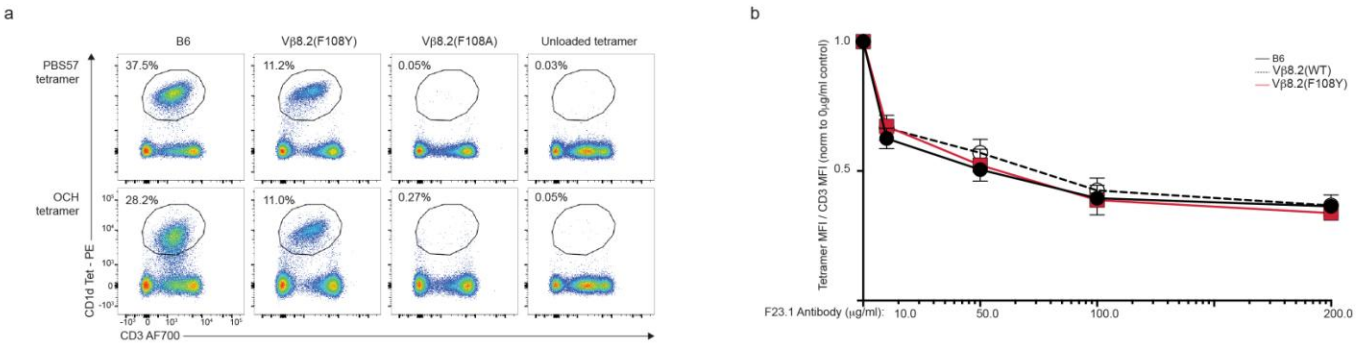

Supplementary Figure 4

The binding kinetics of NKT cell TCRs from B6, V_β8.2(WT), V_β8.2(F108Y) and V_β8.2(F108A) mice are similar.

(**a**) DAPI$^-$MHC II$^-$ hepatocyte populations from B6, V_β8.2(F108Y), and V_β8.2(F108A) mice analyzed by flow cytometry for binding to PBS57-loaded (top row) and OCH-loaded (bottom row) CD1d tetramer. (**b**) FACS analysis of autoMACS-sorted CD1d:PBS57 tetramer$^+$ hepatocytes incubated with 0μg/ml, 10μg/ml, 100μg/ml and 200μg/ml αVβ8 blocking antibody (F23.1) concentrations for two hours at room temperature then analyzed by flow cytometer for tetramer binding levels. Data shown represents the MFI of CD1d Tet (PE) divided by the MFI of CD3 (AF700) normalized to untreated sample (*n*= 3). Data derived from three individual experiments analyzing a combined three biological replicates (mean ±s.e.m. in **b**).

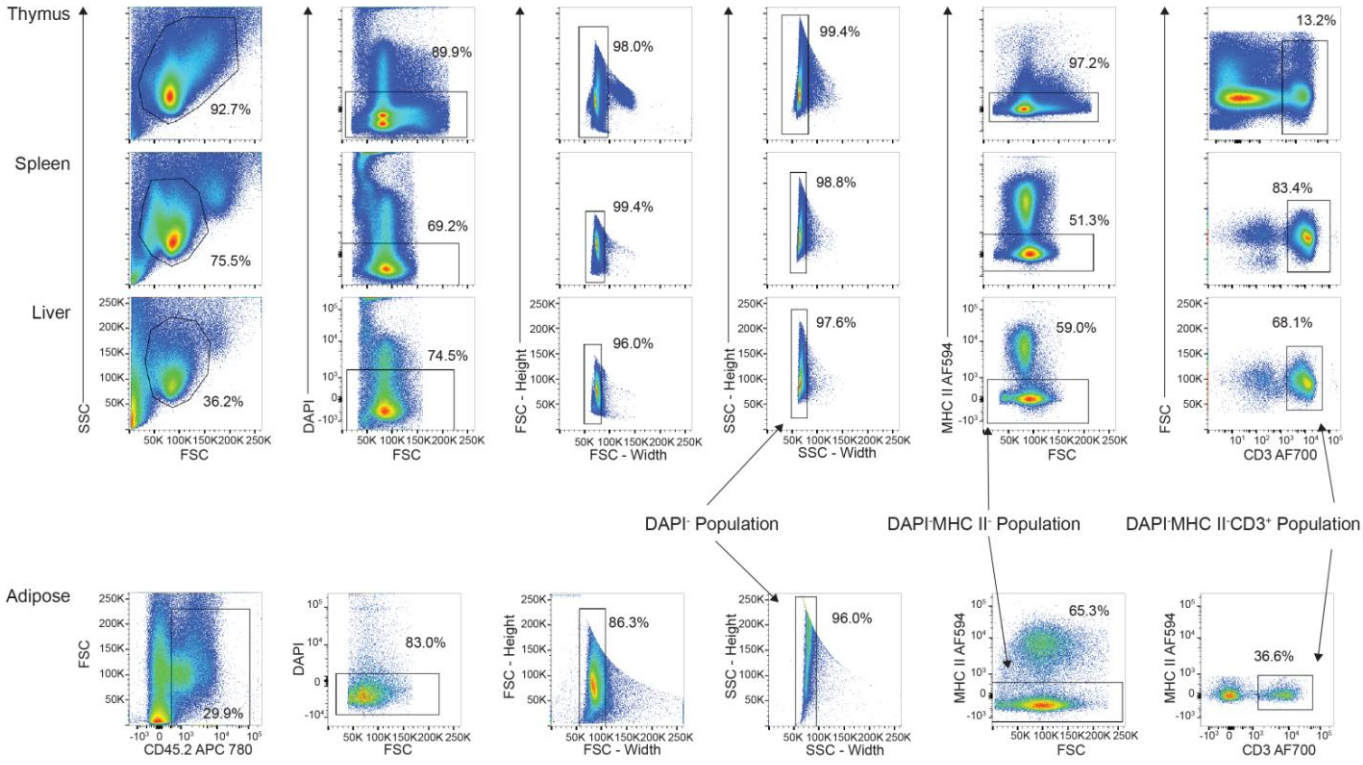

Supplementary Figure 5

Background and preliminary gating strategy for flow cytometry experiments.

Flow cytometry gating strategy for identification of the cell populations discussed in Figures 3-8.